

# Dynamics of Elliptical Galaxies with Planetary Nebulae in Modified Newtonian Dynamics

Yong Tian<sup>1\*</sup> and Chung-Ming Ko<sup>1,2†</sup>

<sup>1</sup>*Institute of Astronomy, National Central University, Zhongli Dist., Taoyuan City, Taiwan (Republic of China)*

<sup>2</sup>*Department of Physics and Center for Complex Systems, National Central University, Zhongli Dist., Taoyuan City, Taiwan (Republic of China)*

Accepted 2016 July 12. Received 2016 July 7; in original form 2016 April 30

## ABSTRACT

The dynamics of an elliptical galaxy within a couple of effective radii can be probed effectively by stars. However, at larger distances planetary nebulae (PNe) replace stars as the tracer of the dynamics. Making use of the motion of PNe, Romanowsky et al. (2003) measured the dynamics of three luminous elliptical galaxies (NGC821, NGC3379 and NGC4494) at large distances from the galactic center. They found that little dark matter is needed up to 6 effective radii. Milgrom & Sanders (2003) showed that this result can be understood in the framework of MODified Newtonian Dynamics (MOND). As more data are available in the past decade, we revisit this problem. We combine PNe data (up to 6–8 effective radii) and stellar data from SAURON of 7 elliptical galaxies, including those 3 galaxies in Romanowsky et al. (2003) with updated data and 4 other galaxies which have not been analyzed before. We conclude that the dynamics of these galaxies can be well explained by MOND.

**Key words:** dark matter – galaxies: elliptical and lenticular, cD – galaxies: kinematics and dynamics – gravitation – gravitational lensing: strong

## 1 INTRODUCTION

The so called “missing mass problem” has been a long standing issue in astrophysics. It was first mentioned by Zwicky (1933) that the gravitational mass inferred by virial theorem was larger than the luminous mass in Coma cluster. However, not until four decades later after the discovery of the flat rotation curve of spiral galaxies (e.g., Rubin & Fort 1970), did scientists took this problem seriously. Now it “appears” everywhere: from galaxies, to cluster of galaxies, and even to cosmological scale phenomena such as large scale structure and cosmic microwave background radiation.

In elliptical galaxies, the “missing mass problem” were found later by different methods such as gravitational lensing, x-ray emission of hot gas, and kinematics of matter. Gravitational lensing is a relativistic phenomenon predicted by General Relativity (GR), which has been tested successfully in the solar system. For large objects such as galaxies or clusters of galaxies, observations showed that the deflection angle of light ray is larger than the prediction of GR. This discrepancy is usually interpreted as dark matter in lens galaxies. Moreover, the Hubble constant  $H_0$  obtained from gravitational time-delay in GR is larger than the value from supernova measurement (Riess et al. 2011). X-ray emitting

hot gas can be used to estimate the gravitational potential of elliptical galaxies, in particular for those in the center of clusters. One can use stellar kinematics to estimate the mass of elliptical galaxies. However, stars are usually concentrated within one effective radius,  $R_{\text{eff}}$ , and this makes the study of dynamics by stars at large distances very difficult. In order to study the dynamics of the galaxy up to several  $R_{\text{eff}}$ , luminous objects such as, planetary nebulae (PNe), globular cluster, or satellite galaxies, are needed.

Romanowsky et al. (2003) reported the dynamics of elliptical galaxies by studying PNe up to 4–6  $R_{\text{eff}}$ . Surprisingly, little dark matter were found contained in the three luminous elliptical galaxies (NGC 821, NGC 3379, NGC 4494) and the data is close to the model by Newtonian dynamics. The “lack of dark matter” can be explained by another view of the “missing mass problem”. The crux of the matter is “mismatch in acceleration”. This can be explained by unseen mass or modified theory of gravity. Milgrom & Sanders (2003) showed that those luminous elliptical galaxies reported by Romanowsky et al. (2003) can be well explained by Modified Newtonian Dynamics (MOND). They pointed out that the systems belong to small acceleration discrepancy in MOND.

With accumulating PNe data for elliptical galaxies in the past decade, we study the dynamics in 7 galaxies in the framework of MOND. The article is organized as follows. After a brief introduction of MOND in Section 2, we present

\* E-mail: yongtian@astro.ncu.edu.tw

† E-mail: cmko@astro.ncu.edu.tw

the data of the elliptical galaxies in Section 3. We describe the mass model and dynamics in Section 4. Result and discussion are provided in Section 5.

## 2 MOND

The “missing mass problem” is, in fact, the mismatch between the measured gravitational acceleration and the inferred Newtonian gravitational acceleration (or GR) produced by the observed luminous matter of the system. The mismatch can be accounted for by the existence of non-luminous matter (a.k.a. dark matter), modified law of inertia or modified theory of gravity. Milgrom (1983) proposed MOND as a modification of Newton’s second law when the acceleration is small than a small constant,  $a_0 \approx 1.2 \times 10^{-10} \text{ m s}^{-2}$ . It turned out that MOND can be expressed as a modified theory of gravity in the form of a nonlinear Poisson equation (Bekenstein & Milgrom 1984),

$$\nabla \cdot [\tilde{\mu}(x)\mathbf{g}] = \nabla \cdot \mathbf{g}_N = -4\pi G\rho, \quad (1)$$

where  $\mathbf{g}$  is the gravitational acceleration in MOND,  $\mathbf{g}_N$  the gravitational acceleration in Newtonian gravity, and  $x = |\mathbf{g}|/a_0$ .  $\tilde{\mu}(x)$  is called the interpolation function. It has the asymptotic behavior  $\tilde{\mu}(x) \approx 1$  for  $x \gg 1$  (Newtonian regime) and  $\tilde{\mu}(x) \approx x$  for  $x \ll 1$  (deep MOND regime). Chiu et al. (2011) suggested a canonical interpolation function of the following form

$$\tilde{\mu}(x) = \left[ 1 - \frac{2}{(1 + \eta x^\alpha) + \sqrt{(1 - \eta x^\alpha)^2 + 4x^\alpha}} \right]^{1/\alpha}. \quad (2)$$

From the kinematics of matter, MOND not only successfully explained the mass discrepancy (or the mismatch of acceleration) in spiral galaxies (Sanders & McGaugh 2002), but also the baryonic Tully-Fisher relation (McGaugh 2011) in large acceleration mismatch systems. Recently, there are some studies on the kinematics of elliptical galaxies related to MOND, e.g., Rodrigues (2012), Tortora et al. (2014).

Relativistic effects such as gravitational lensing and time-delay can be studied under a relativistic gravity theory of MOND, e.g., TeVeS, GEA or BiMOND (Bekenstein 2004; Zlosnik et al. 2007; Milgrom 2009). Chiu et al. (2006) was the first to derive the gravitational lensing equation in relativistic MOND rigorously from TeVeS. This has been well tested on elliptical galaxy lens in quasar lensing (see, e.g., Zhao 2006; Chiu et al. 2011) and also for quasar time-delay systems (Tian et al. 2013). In most quasar lensing cases, the system acceleration of the elliptical galaxy lenses is around  $1 \sim 10 a_0$ , and small acceleration discrepancy is expected. Sanders (2014) also tested strong lensing in MOND on the Sloan Lens Advanced Camera Surveys samples of elliptical lens to get a luminous mass consistent with stellar mass determined from population synthesis models using Salpeter initial mass function (IMF).

Hot gas in elliptical galaxies emit x-ray. Milgrom (2012) found that MOND fitted well with the data from NGC 720 and NGC 1521 to very large galactic radii (100 and 200 kpc), which correspond to a wide range of acceleration from  $0.1 a_0$  to more than  $10 a_0$ . In addition, globular clusters can be used to study the dynamics of elliptical galaxies outside several effective radii in MOND (see, e.g., Richtler et al. 2008; Samurović & Ćirković 2008; Schuberth et al. 2012;

Samurović 2012, 2014). Samurović (2014) pointed out that although MOND is successful in explaining the dynamics of less massive fast rotators, it cannot fit several massive slow rotators well without an additional dark matter.

A convenient parameter

$$\xi \equiv \left( \frac{GM}{R_{\text{eff}}^2 a_0} \right)^{1/2}, \quad (3)$$

has been used to distinguish between different regimes, say, Newtonian and deep MOND regimes (Milgrom 1983; Milgrom & Sanders 2003). For spiral galaxies in deep MOND regime, the terminal velocity is given by  $V_\infty^2 = \sqrt{GM a_0}$ , and Equation (3) can be expressed as  $\xi = V_\infty^2 / (R_{\text{eff}} a_0)$  (Milgrom 1983). Equivalently, instead of Equation (3), one can define a critical surface density  $\Sigma_c = a_0/G$  (Milgrom & Sanders 2003).

In the case of spiral galaxies,  $\xi > 1$  and  $\xi < 1$  (or  $\Sigma > \Sigma_c$  and  $\Sigma < \Sigma_c$ ) correspond to high surface brightness (HSB) spirals and low surface brightness (LSB) spirals, respectively. In the framework of dark matter, HSB spirals require less dark matter while LHS spirals more. In the framework of MOND,  $\xi$  tells us the whether the system is more like a Newtonian system (HSB when  $\xi > 1$ ) or a MONDian system (LSB when  $\xi < 1$ ).

In the case of elliptical galaxies, let us take the three galaxies in Romanowsky et al. (2003) as examples. Milgrom & Sanders (2003) estimated luminous the masses by assuming mass-to-light ratio equal to 4, and got  $\xi \approx 5.7$  for NGC 3379,  $\xi \approx 3.6$  for NGC 821 and  $\xi \approx 3.4$  for NGC 4494.

## 3 DATA

As the surface brightness from the stars of elliptical galaxies drops rapidly beyond  $2 R_{\text{eff}}$ , the kinematics of the galaxy at larger distances has to be studied by other sources. Motion of gas can be used in spiral galaxies but this is not suitable for elliptical galaxies as their gas content is low. Instead, planetary nebulae (PNe) and globular clusters have been suggested for elliptical galaxies. PNe are good tracers for velocity distribution because of their strong emission line O[III] at 500.7 nm.

The first PN radial velocity measurement was made in the halo of Centaurus A at the Anglo-Australian Telescope (Hui et al. 1995) by using a multi-fiber instrument. The success of the project led to a special-purpose instrument, the Planetary Nebulae Spectrograph (PN.S) mounted on the William Herschel Telescope in La Palma (Douglas et al. 1997).

The PN.S (Douglas et al. 2002) split the incoming light into two separate cameras and was able to measure simultaneously the position, radial velocity and flux of the PNe in the target galaxies. Since its first-light in 2001, PN.S focused on elliptical S0 galaxies. Its data is publicly available in PN.S public website<sup>1</sup>. Its catalogue lists positions, observed wavelength, heliocentric radial velocity, and magnitude of PNe (Douglas et al. 2007; Coccato et al.

<sup>1</sup> [http://www.strw.leidenuniv.nl/pns/PNS\\_public\\_web](http://www.strw.leidenuniv.nl/pns/PNS_public_web)

Table 1. The sample of elliptical galaxies.

Name	Type	D Mpc	$V_{\text{los}}$ $\text{km s}^{-1}$	$M_B$ mag	$N_{\text{PNe}}$	$R_{\text{eff}}$ arcsec	$R_{\text{last}}$ arcmin	References
(1)	(2)	(3)	(4)	(5)	(6)	(7)	(8)	(9)
NGC 821	E6	23.4	1718	-20.81	127	39.8	6.8	Coccato et al. (2009)
NGC 1344	E5	18.4	1169	-19.66	194	46	6.7	Coccato et al. (2009)
NGC 3379	E1	10.3	918	-20.67	214	39.8	7.2	Douglas et al. (2007)
NGC 4374	E1	18.5	1017	-21.21	454	52.5	6.9	Coccato et al. (2009)
NGC 4494	E1	16.6	1342	-21.12	267	50	7.6	Napolitano et al. (2009)
NGC 4697	E6	11.4	1252	-21.22	535	61.7	6.6	Coccato et al. (2009)
NGC 5846	E0	24.2	1712	-21.33	124	58.9	6	Coccato et al. (2009)

Notes. (1) name of galaxy, (2) morphological type of galaxy in NED, (3) distance from ATLAS<sup>3D</sup> (Cappellari et al. 2011), (4) galaxy heliocentric systemic velocity in NED, (5) absolute B-band magnitude from HyperLeda database (Makarov et al. 2009), (6) total number of PNe with measured radial velocities from Coccato et al. (2009), (7) effective radius from ATLAS<sup>3D</sup> database (Cappellari et al. 2011), (8) maximum distance of the PNe detections from the galaxy center (Coccato et al. 2009), (9) reference of the PNe data.

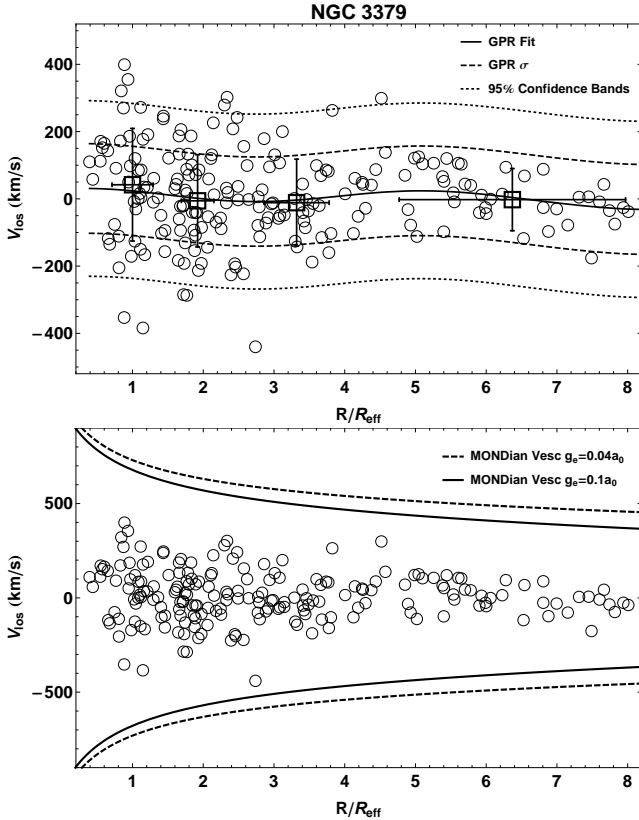


**Figure 1.** Upper panel: Line-of-sight velocity of 214 PNe in NGC 3379 (circles) is plotted against their distance from the galactic center (data from PN.S public website). The four squares are the average line-of-sight velocity from maximum likelihood, and the vertical error bar represents the line-of-sight velocity dispersion. The solid line is the mean velocity obtained by Gaussian Process Regression (GPR). The dash line and the dotted line are the error and 95% confidence band by GPR, respectively. Lower panel: escape speed of a test particle in NGC 3379. Due to the external field effect, particles can escape a MONDian system if the system is embedded in a constant external field (see, e.g., Bekenstein & Milgrom 1984; Famaey et al. 2007). The solid line is the escape speed for an external field  $0.1a_0$  and dash line for  $0.04a_0$ . Simple form is used in this example.

2009; Napolitano et al. 2009). The PNe line-of-sight velocity distribution of NGC 3379 is shown in the upper panel of Figure 1. The velocity dispersion of NGC 3379 is obtained from the distribution by maximum likelihood method for 4 bins. This is consistent with the analysis by Gaussian Process Regression, see upper panel of Figure 1. We also obtain the velocity dispersion of NGC 4494 and NGC 821 by the same procedure. For NGC 5846, NGC 4374, NGC 1344 and NGC 4697 we take the values published in SAURON (Coccato et al. 2009).

For illustration we plot the escape speed of a test particle in NGC 3379. Recall that the MONDian potential at large distance from a galaxy (a finite object) is  $\sim \log r$ , thus every test particle is bound. However, if the galaxy is embedded in a constant external field  $\mathbf{g}_e$ , the test particle can escape due to the external field effect in MOND (see, e.g., Bekenstein & Milgrom 1984; Famaey et al. 2007; Famaey & McGaugh 2012). Adopting the procedure of Famaey et al. (2007), and choosing simple form ( $\mu(x) = x/(1+x)$ ), we have (cf. Equation (5) of Famaey et al. 2007)

$$\frac{g(g + g_e)}{g + g_e + a_0} = \frac{Gm(r)}{r^2} = g_N, \quad (4)$$

where  $g = |\mathbf{g}|$ ,  $g_e = |\mathbf{g}_e|$ , and  $m(r)$  is the mass enclosed within  $r$ . The escape speed can be computed from

$$v_{\text{esc}}(R) = \left[ 2 \int_R^\infty g(r) dr \right]^{1/2}. \quad (5)$$

We adopt Hernquist model for the mass distribution, i.e.,  $m(r) = Mr^2/(r + r_h)^2$ , where we use the Salpeter mass for  $M$  (Cappellari et al. 2013a,b). The lower panel of Figure 1 shows the escape speed of two cases:  $g_e = 0.1a_0$  and  $0.04a_0$ .

For the stellar component, SAURON integral-field unit on the William Herschel Telescope has produced excellent two dimensional velocity dispersion data of nearby elliptical galaxies (Coccato et al. 2009). By folding the major axis and the minor axis components (e.g., Romanowsky et al. 2003), we combine the data from stellar component with data from PNe component to study the dynamics of the sample galaxies up to several  $R_{\text{eff}}$ .

There are 16 galaxies with publicly available PNe data

posted in the P.N.S public website. Among these, 8 are classified as S0 and 8 elliptical galaxies. In this work, we focus on elliptical galaxies only. The elliptical galaxy NGC 4283 has only 11 PNe data which is not enough for our analysis. Thus we have 7 elliptical galaxies in our sample: NGC 821, NGC 1344, NGC 3379, NGC 4374, NGC 4494, NGC 4697, and NGC 5846. Table 1 lists some properties of these galaxies.

## 4 MODEL

For simplicity, we model an elliptical galaxy as a spherically symmetric stellar system.

### 4.1 Velocity dispersion

The velocity dispersion a spherically symmetric stellar system in equilibrium is governed by the Jeans equation in spherical coordinates (see, e.g., Binney & Tremaine 2008),

$$\frac{d(\rho\sigma_r^2)}{dr} + \frac{2\beta}{r}\rho\sigma_r^2 = -\rho g, \quad (6)$$

where  $\beta = 1 - (\sigma_t^2/\sigma_r^2)$  is the anisotropy parameter ( $\beta = 0$  for the isotropy case).

The velocity dispersion measured along the line-of-sight at projected radius  $R$  is given by

$$\sigma_I^2(R) = \frac{2}{I(R)} \int_R^\infty \sigma_r^2 \left(1 - \beta(r) \frac{R^2}{r^2}\right) \frac{\rho(r)rdr}{\sqrt{r^2 - R^2}}, \quad (7)$$

where the surface density is

$$I(R) = 2 \int_R^\infty \frac{\rho(r')r' dr'}{\sqrt{r'^2 - R^2}}. \quad (8)$$

In this paper we consider isotropic model (i.e.,  $\beta = 0$ ) and a particular anisotropic model

$$\beta = \frac{r^2}{r_a^2 + r^2}. \quad (9)$$

This anisotropic model can be formed by dissipationless collapse systems (see, e.g., van Albada 1982; Milgrom & Sanders 2003).

### 4.2 Mass model

We adopt Hernquist profile (Hernquist 1990) as the mass model for the elliptical galaxies,

$$\rho_h(r) = \frac{M_h r_h}{2\pi r(r + r_h)^3}, \quad g_h(r) = \frac{G M_h}{(r + r_h)^2}, \quad (10)$$

where  $M_h$  is the mass of the galaxy and  $g_h$  is the corresponding Newtonian gravitational acceleration. We note again that we take the convention that positive gravitational acceleration means towards the origin. Assuming constant mass-to-light ratio, the surface brightness distribution is the same as the surface density distribution, and the effective radius  $R_{\text{eff}}$  is the same as half-mass radius. In this case,  $r_h \approx 0.551 R_{\text{eff}}$  and this is the relation we use in our modeling.

As stellar data in the innermost region indicates the

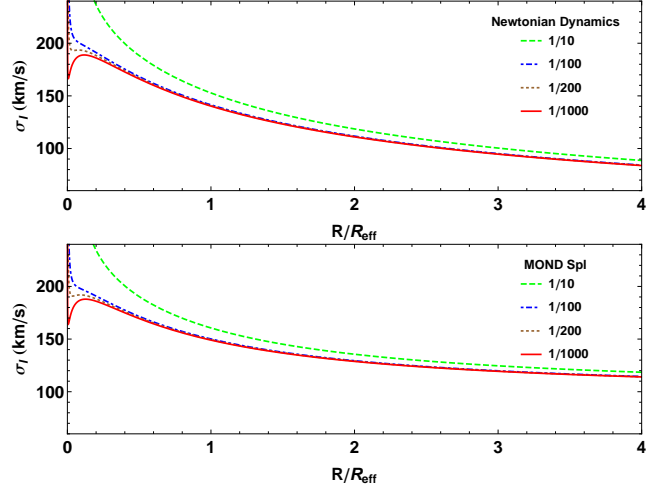


**Figure 2.** The projected line-of-sight velocity dispersion profile of a galaxy. The mass distribution of the galaxy is described by Hernquist model. Newtonian gravity and simple form in MOND are used as the examples. Besides the self-gravity of the mass distribution, the influence of a SMBH at the center is considered. The dash line represents SMBH to galaxy mass ratio at 1/10, dotted-dash line at 1/100, dotted line at 1/200, and solid line at 1/1000. (Color in online version: dash, dotted-dash, dotted and solid correspond to green, blue, orange and red, respectively.)

need of a supermassive black hole (SMBH), we also include a point mass at the center to represent the SMBH

$$g_{\text{bh}}(r) = \frac{GM_{\text{bh}}}{r^2}. \quad (11)$$

Figure 2 shows the effect of a SMBH in a Hernquist model on velocity dispersion. Different curves in the figure represent different SMBH mass to galaxy mass ratio ( $M_{\text{bh}}/M_h$ ). In our sample, this ratio is within the range 1/700 – 1/200. For mass ratio less than 1/100 ( $M_{\text{bh}}/M_h < 1/100$ ), the effect of the SMBH can be seen within  $0.2 R_{\text{eff}}$  only.

We use simple singular isothermal model for the dark matter halo when we compared MOND and Newtonian gravity of the galaxies later,

$$g_{\text{iso}}(r) = \frac{2\sigma_v^2}{r}. \quad (12)$$

### 4.3 Gravity model

We adopt MOND for the gravitational acceleration in Section 4.1. For spherically symmetric systems, Equation (1) can be “inverted” to

$$\mathbf{g} = -g \hat{\mathbf{e}}_r = \tilde{\nu}(x_N) \mathbf{g}_N = -\tilde{\nu}(x_N) g_N \hat{\mathbf{e}}_r, \quad (13)$$

where  $x_N = |\mathbf{g}_N|/a_0 = g_N/a_0$  and  $\tilde{\nu}(x_N)$  is called the inverted interpolation function. The canonical form of this function can be obtained from Equation (2) (see, Chiu et al. 2011),

$$\tilde{\nu}(x_N) = \left[1 + \frac{1}{2} \left(\sqrt{4x_N^{-\alpha} + \eta^2} - \eta\right)\right]^{1/\alpha}. \quad (14)$$

For instance, in this paper we use (1)  $(\alpha, \eta) = (2, 1)$ , where Equation (2) becomes  $\tilde{\mu}(x) = x/\sqrt{1+x^2}$  and is called the standard form (e.g., Milgrom 1983), and (2)  $(\alpha, \eta) = (1, 1)$ ,



where  $\tilde{\mu}(x) = x/(1+x)$  and is called the simple form (e.g., Famaey & Binney 2005).

To compute the velocity dispersion  $\sigma_I$  in Equation (7), we adopt the mass distribution  $\rho_h$  of the Hernquist model in Equation (10). In addition to the self-gravity of the mass distribution, the gravitational acceleration on the system may consist of a contribution from a central SMBH. To compute the gravitational acceleration in MOND we set  $g_N = g_h + g_{bh}$  and then use Equation (13) to get  $g$  for Equation (7). For comparison, we also compute the Newtonian gravitational acceleration with a dark matter halo, i.e.,  $g = g_N = g_h + g_{iso}$ .

## 5 RESULT AND DISCUSSION

In dark matter halo scenario, one expects that close to the center of a galaxy ordinary matter dominates dark matter, while at large distances from the center dark matter becomes dominant. Thus measurement of the dynamics at the outskirts of galaxies is crucial to dark matter scenario. As an alternative to dark matter scenario, MOND predicts the dynamics at the outskirts solely by the ordinary matter of the galaxy. We use PN.S data to trace the dynamics of 7 elliptical galaxies (see Table 1) up to 6–8 effective radii. Besides, we also use stellar data from SAURON (Coccato et al. 2009) and ATLAS<sup>3D</sup> (Cappellari et al. 2011) to constraint the model at smaller radii.

We adopt a spherically symmetric Hernquist model for these galaxies and allow for a SMBH at the center. We choose two interpolation functions in MOND in our study: standard form and simple form ( $(\alpha, \eta) = (2, 1)$  and  $(1, 1)$  in Equation (14)). Moreover, we choose the acceleration parameter in MOND from the baryonic Tully-Fisher relation (McGaugh 2011), i.e.,  $a_0 = 1.21 \times 10^{-10} \text{ m s}^{-2}$ . The characteristic length scale  $r_h$  is presumably provided by observed  $R_{\text{eff}}$  via  $r_h \approx 0.551 R_{\text{eff}}$ . We thus have a two-parameter model (one for the mass of the galaxy  $M_h$  and the other the mass of the SMBH  $M_{bh}$ ), and if the mass of the SMBH is given then we have a one-parameter model. For comparison we also study dark matter scenario, in which we include an additional isothermal dark matter halo in Newtonian gravity (this is a two-parameter model, the mass of the galaxy  $M_h$  and  $\sigma_v$  of the halo).

The mass of the SMBH of 4 elliptical galaxies (NGC 4697, NGC 821, NGC 3379 and NGC 4374) in our sample has been measured by other method (McConnell et al. 2011). With a prescribed mass for the SMBH, we have only one parameter in our model for MOND, the mass of the galaxy  $M_h$ . The result of the fitting by reduced  $\chi$ -square is shown in Figure 3.

Four models are shown in the figure:

- (1) dotted-dash line: Hernquist model with SMBH in MOND in simple form;
- (2) solid line: Hernquist model with SMBH in MOND in simple form with anisotropic parameter  $\beta$  in Equation (9),
- (3) dotted line: Hernquist model with SMBH in Newtonian gravity;
- (4) dash line: Hernquist model with isothermal dark matter halo (but without SMBH) in Newtonian gravity.

The first three are one-parameter models and the last one is a two-parameter model. The numerical values of the fitting

parameter and the corresponding errors by reduced  $\chi$ -square method are shown in Table 2 (also Table 4). The table also lists the mass estimated by population synthesis. From the table, we learn that, except NGC 821, the mass of other three elliptical galaxies matches well with the population synthesis model based on Salpeter IMF (Cappellari et al. 2013b). We point out that the statistics of NGC 821 is not very good due to insufficient stellar and PN data.

When we let the mass of the SMBH as a free parameter, our model for MOND becomes a two-parameter model. There are 5 galaxies in our sample suitable for the analysis (NGC 3379, NGC 4374, NGC 5846, NGC 1344 and NGC 4494). NGC 4697 and NGC 821 are not included because of the lack of stellar data in the inner region close to the center. We fit the data by reduced  $\chi$ -square and Figure 4 shows the result of the 5 galaxies. Four models are shown in the figure. The four models are the same as in Figure 3 except that all four models are two-parameter models. The numerical values of the fitting parameters and the corresponding errors by reduced  $\chi$ -square method are listed in Table 3 and Table 4. From the table, we notice that the SMBH mass of NGC 3379 and NGC 4374 are consistent with the observed values (McConnell et al. 2011).

Our sample includes the three galaxies, NGC 821, NGC 3379 and NGC 4494, studied by Romanowsky et al. (2003). In the past decade observation has improved a lot. There are about twice as many PNe data (Coccato et al. 2009) and better measurement in distance and effective radius are obtained by ATLAS<sup>3D</sup> (Cappellari et al. 2011). Our results and those of Romanowsky et al. (2003) and Milgrom & Sanders (2003) on the three galaxies are consistent with each other. Table 5 gives a detail comparison. Moreover, analysis on four other galaxies (NGC 4374, NGC 5846, NGC 1344 and NGC 3377) renders similar conclusion as in Romanowsky et al. (2003), Newtonian dynamics is close to data of velocity dispersion within 6 effective radius. This runs into the tenet of dark matter halo models which are supposed to have more dark matter at the outer part of galaxies.

Hernquist model in MOND fits the data well (see Figures 3 & 4 and Table 4). The existence of a SMBH has almost no influence on the dynamics at distances beyond one effective radius (the same conclusion as the case for pure Newtonian gravity discussed in Section 4.2, see Figure 2). In our samples, different interpolation functions (such as simple form and standard form) only produce very small difference in the profile of the velocity dispersion and give very similar best fit parameters.

All the masses of the galaxies found under MOND are at most 17% less than those found under Newtonian gravity. The mass discrepancy is small because the “effective acceleration” is large comparing with  $a_0$ , the acceleration parameter of MOND, thus the systems are closer to Newtonian regime. Recall the parameter  $\xi$  from Equation (3)  $\xi = \sqrt{GM/R_{\text{eff}}^2 a_0}$ . We calculate  $\xi$  by taking the mass estimated by population synthesis with Salpeter IMF and the effective radius in ATLAS<sup>3D</sup> (Cappellari et al. 2011), and choose  $a_0 = 1.21 \times 10^{-10} \text{ m s}^{-2}$  (McGaugh 2011). We list  $\xi$  and the mass (from Newtonian gravity and MOND) in Tables 2 and 3. All of them are larger than unity ( $\xi \sim 2.7$  to 5.3), cf. HSB spiral galaxies (see the end of Section 2). Large  $\xi$  is indicative of system close to Newtonian regime,

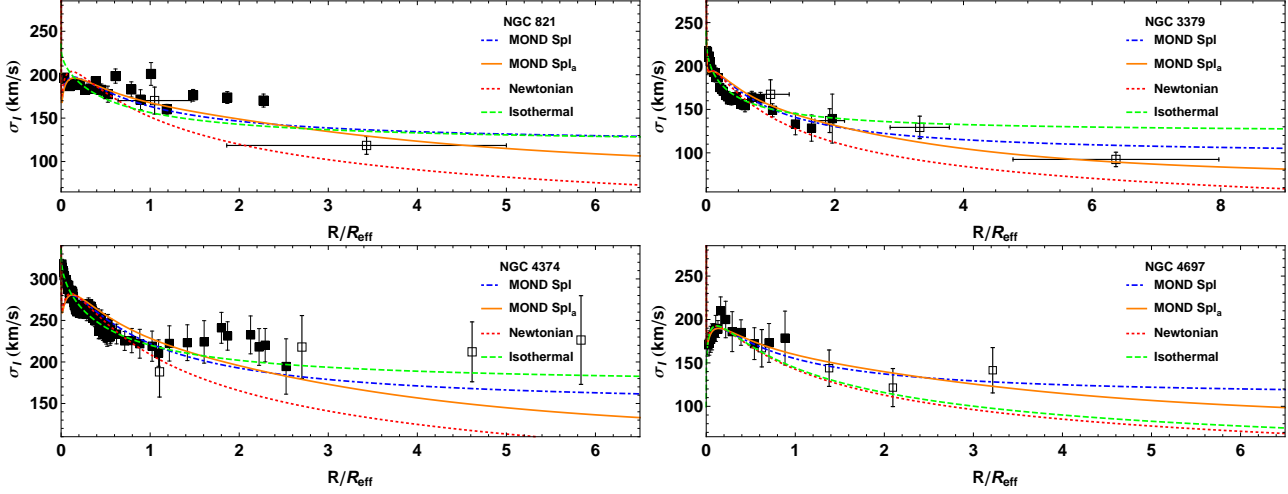


**Figure 3.** The projected line-of-sight velocity dispersion of NGC 4697, NGC 821, NGC 3379 and NGC 4374 (see Table 1) as a function of the projected radius normalized to  $R_{\text{eff}}$  of individual galaxy. Open circles are PNe data and solid circles are stellar data. Dotted-dash line and solid line correspond to MOND, and dashed line and dotted line to Newtonian gravity. Dotted-dash line is the best fit of Hernquist isotropic model with SMBH in MOND in simple form in Equation (14). Solid line is the same as dotted-dash line except that it is an anisotropic model with  $r_a = 3R_{\text{eff}}$  (see Equation (9)). Dotted line is Hernquist model with SMBH (but without dark matter halo) in Newtonian gravity. Dash line is the best fit of Hernquist model with isothermal dark matter halo in Newtonian gravity. The masses of the SMBH for the solid line, dotted-dash line and the dotted line are prescribed and their values are adopted from McConnell et al. (2011). Each of these three lines is the result of one-parameter fitting, the mass of the galaxy  $M_h$ , while the dash line is the result of two-parameter fitting, the mass of the galaxy  $M_h$  and the parameter of the singular isothermal sphere  $\sigma_v$ , see Table 2. (Color in online version: dotted-dash, solid, dotted and dash correspond to blue, red, orange and green, respectively.)

**Table 2.** The fitting parameters of Figure 3.

Name	$M_h$	$M_{\text{dm}(<5R_{\text{eff}})}$	$M_h$	$M_h$	$M_h$	$M_{\text{bh}}$	$M_{\text{Sal}}$	$\xi$
	Iso	Iso	New	Spl <sub>a</sub>	Spl		Sal	
(1)	(2)	(3)	(4)	(5)	(6)	(7)	(8)	(9)
NGC 821	$7.0 \pm 1.7$	$29.8^{+3.16}_{-3.0}$	$23.3 \pm 0.34$	$19.6 \pm 0.32$	$20.3 \pm 0.33$	$1.8^{+0.8}_{-0.8}$	11.1	2.7
NGC 3379	$1.8 \pm 0.28$	$13.9^{+0.46}_{-0.45}$	$8.9 \pm 0.08$	$8.4 \pm 0.07$	$8.6 \pm 0.08$	$4.6^{+1.1}_{-1.2}$	11.1	5.1
NGC 4374	$13.2 \pm 0.90$	$63.8^{+1.64}_{-1.61}$	$46.2 \pm 0.21$	$43.1 \pm 0.20$	$43.7 \pm 0.21$	$8.5^{+0.9}_{-0.8}$	41.1	5.0
NGC 4697	$15.0 \pm 2.92$	$1.67^{+8.22}_{-1.35}$	$15.6 \pm 0.66$	$14.0 \pm 0.64$	$14.3 \pm 0.65$	$2.0^{+0.2}_{-0.2}$	14.6	3.7

*Notes.* (1) name of galaxy, (2) fitting luminous mass of the galaxy, (3) fitting mass of dark matter halo within 5 effective radii, (4) fitting mass of the galaxy in Newtonian gravity, (5) fitting mass of the galaxy in MONDian gravity in simple form with anisotropic parameter  $\beta$ , (6) fitting mass of the galaxy in MONDian gravity in simple form, (7) mass of the SMBH (in  $10^8 M_\odot$ ) from McConnell et al. (2011), (8) mass estimated from population synthesis models with Salpeter IMF (ATLAS<sup>3D</sup>, Cappellari et al. 2013a,b), (9) the parameter  $\xi$  in Equation (3) with mass given by column (8). All masses are in unit of  $10^{10} M_\odot$  (except mass of SMBH). Columns (2) & (3) are the results of two-parameter fitting in Newtonian gravity (luminous mass  $M_h$  and parameter of the isothermal dark matter halo  $\sigma_v$ ). Columns (4), (5) & (6) are the results of one-parameter fitting (galaxy mass  $M_h$  with the mass of the SMBH given by Column (7)).

and therefore, the difference in masses found by Newtonian theory and MOND is expected to be small.

To compare with dark matter model, we consider a Hernquist model for the galaxy and a singular isothermal sphere for the dark matter halo in Newtonian gravity. The dark matter model can fit the data as well. However, for some cases such as NGC 3379, NGC 4374 and NGC 4494, the baryonic mass of the galaxy is a lot less than expected from population synthesis models with Salpeter IMF, see Tables 2 and 3. Within the dark matter halo model five galaxies (NGC 821, NGC 3379, NGC 4374, NGC 5846 and NGC 1344) have dark halo mass  $M_{\text{dm}}$  (mass of dark matter within  $5R_{\text{eff}}$ ) significantly larger than the baryonic mass  $M_h$ .

However, these  $M_{\text{dm}}$  are not much larger than the Salpeter mass. We would like to point out that NGC 4697 has negligible dark matter and the best fit is very close to the model without dark halo (see Figure 3). In Table 4, one notices that the mass-to-light ratios of NGC 3379, NGC 4374, NGC 1344 and NGC 4494 are too small for common dark matter model.

In addition, our work confirms two predictions by MOND: (1) mass discrepancy increases as Newtonian acceleration decreases (McGaugh 2004; Famaey & McGaugh 2012), and (2) maximum halo acceleration (Milgrom & Sanders 2005; Gentile et al. 2009).

Mass discrepancy refers to the ratio of the dynamical mass to the baryonic mass. Usually it is represented by

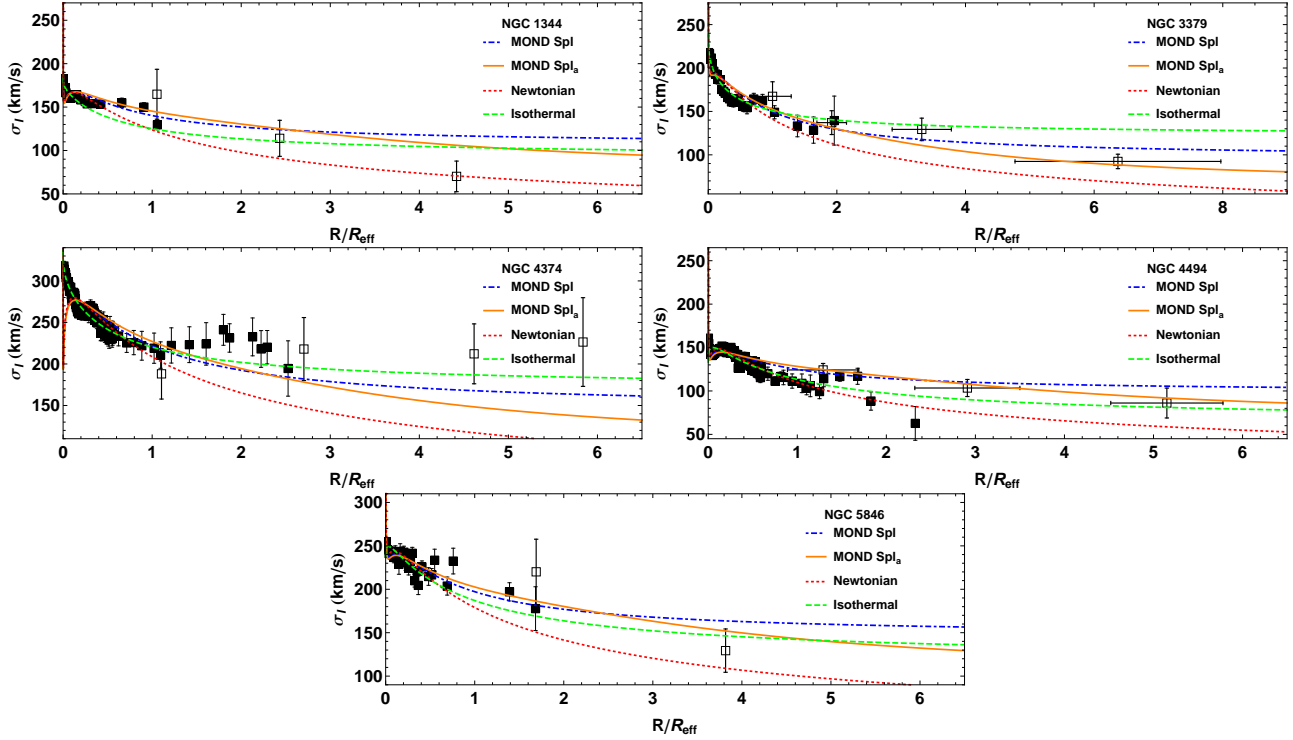


**Figure 4.** The same as Figure 3 but for the galaxies NGC 1344, NGC 3379, NGC 4374, NGC 4494, and NGC 5846. All the lines are the result of two-parameter fitting. The fitting parameters for dotted-dash line, solid line, and dotted line are the mass of the galaxy and SMBH ( $M_h$  and  $M_{bh}$ ), see Table 3. Dash line is the same as in Figure 3, i.e.,  $M_h$  and  $\sigma_v$ . (Color in online version: dotted-dash, solid, dotted and dash correspond to blue, red, orange and green, respectively.)

**Table 3.** The fitting parameters of Figure 4.

Name	$M_h$	$M_{dm(<5R_{eff})}$	$M_h$	$M_{bh}$	$M_h$	$M_{bh}$	$M_h$	$M_{bh}$	$M_{bh}$	$M_{Sal}$	$\xi$
	Iso	Iso	New	New	Spl <sub>a</sub>	Spl <sub>a</sub>	Spl	Spl		Sal	
(1)	(2)	(3)	(4)	(5)	(6)	(7)	(8)	(9)	(10)	(11)	(12)
NGC 1344	$4.7 \pm 0.22$	$16.3^{+0.31}_{-0.31}$	$14.1 \pm 0.5$	$2.68 \pm 0.1$	$12.6 \pm 0.5$	$2.77 \pm 0.1$	$12.8 \pm 0.5$	$2.81 \pm 0.1$	—	(16.8)	(5.3)
NGC 3379	$1.8 \pm 0.28$	$13.9^{+0.46}_{-0.45}$	$8.8 \pm 0.6$	$5.19 \pm 0.3$	$8.1 \pm 0.6$	$5.59 \pm 0.4$	$8.4 \pm 0.6$	$5.38 \pm 0.4$	$4.6^{+1.1}_{-1.2}$	11.1	5.1
NGC 4374	$13.2 \pm 0.90$	$63.8^{+1.64}_{-1.61}$	$46.6 \pm 2.1$	$11.1 \pm 0.5$	$42.6 \pm 2.1$	$12.4 \pm 0.6$	$43.7 \pm 2.1$	$11.8 \pm 0.6$	$8.5^{+0.9}_{-0.8}$	41.1	5.0
NGC 4494	$7.0 \pm 0.21$	$7.7^{+0.37}_{-0.36}$	$10.9 \pm 0.3$	$2.29 \pm 0.1$	$8.9 \pm 0.3$	$2.85 \pm 0.1$	$9.3 \pm 0.3$	$2.7 \pm 0.1$	—	12.4	3.0
NGC 5846	$28.0 \pm 0.28$	$44.0^{+3.54}_{-3.40}$	$49.5 \pm 7.6$	$18.9 \pm 2.9$	$42.9 \pm 7.6$	$22.3 \pm 3.9$	$44.3 \pm 7.7$	$21.3 \pm 3.7$	—	32.9	3.3

*Notes.* (1) name of galaxy, (2) fitting luminous mass of the galaxy, (3) fitting mass of dark matter halo within 5 effective radii, (4) fitting mass of the galaxy in Newtonian gravity, (5) fitting SMBH mass in Newtonian gravity, (6) fitting mass of the galaxy in MONDian gravity in simple form with anisotropic parameter  $\beta$ , (7) fitting SMBH mass in MONDian gravity in simple form with anisotropic parameter  $\beta$ , (8) fitting mass of the galaxy in MONDian gravity in simple form, (9) fitting SMBH mass in MONDian gravity in simple form, (10) mass of the SMBH from McConnell et al. (2011), (11) mass estimated from population synthesis models with Salpeter IMF (ATLAS<sup>3D</sup>, Cappellari et al. 2013a,b), (12) the parameter  $\xi$  of Equation (3) with mass given by column (11).  $M_h$  and  $M_{dm}$  are in unit of  $10^{10} M_\odot$  while  $M_{bh}$  in  $10^8 M_\odot$ . Columns (2) & (3) are the results of two-parameter fitting in Newtonian gravity (luminous mass  $M_h$  and parameter of the isothermal dark matter halo  $\sigma_v$ ). Columns (4) & (5) are the results of two-parameter fitting in Newtonian gravity (galaxy mass  $M_h$  and SMBH mass  $M_{bh}$ ). (6) & (7) and (8) & (9) are the same as (4) & (5) except they are the results of MONDian gravity in standard form and simple form, respectively. We note that in the case of NGC 1344, we do not have the mass from population synthesis. Its mass in Column (11) is estimated from its luminosity  $4.2 \times 10^{10} L_\odot$  (Teodorescu et al. 2005) with a mass-to-light ratio equal to 4 (Milgrom & Sanders 2003).

**Table 4.** The fitting parameters for Figure 3 & 4 in term of mass-to-light ratio.

Name	$L_R$	$\Upsilon_{R,h}$ Iso	$\Upsilon_{R,dm+h(<5R_{eff})}$ Iso	$\Upsilon_{R,h}$ New	$\Upsilon_{R,h}$ Spl <sub>a</sub>	$\Upsilon_{R,h}$ Spl	$\Upsilon_{R,Sal}$ Sal
(1)	(2)	(3)	(4)	(5)	(6)	(7)	(8)
NGC 821	1.87	3.74±0.91	23.4 <sup>+2.08</sup> <sub>-1.98</sub>	12.5±0.18	10.5±0.17	10.9±0.18	5.92
NGC 3379	1.62	1.11±0.17	11.7 <sup>+0.35</sup> <sub>-0.34</sub>	5.49±0.05	5.19±0.05	5.31±0.05	6.88
NGC 4374	5.87	2.25±0.15	15.6 <sup>+0.34</sup> <sub>-0.34</sub>	7.87±0.04	7.34±0.04	7.44±0.04	7.01
NGC 4697	2.31	6.49±1.26	7.36 <sup>+4.39</sup> <sub>-0.72</sub>	6.75±0.29	6.06±0.17	6.19±0.28	6.31
NGC 1344	4.2	1.12±0.05	5.90 <sup>+0.09</sup> <sub>-0.09</sub>	3.36±0.12	3.00±0.12	3.05±0.12	—
NGC 3379	1.62	1.11±0.17	11.7 <sup>+0.35</sup> <sub>-0.34</sub>	5.43±0.35	5.00±0.37	5.19±0.35	6.88
NGC 4374	5.87	2.25±0.15	15.6 <sup>+0.34</sup> <sub>-0.34</sub>	7.94±0.36	7.26±0.36	7.44±0.35	7.01
NGC 4494	2.48	2.82±0.08	6.66 <sup>+0.18</sup> <sub>-0.18</sub>	4.40±0.10	3.59±0.12	3.75±0.10	5.0
NGC 5846	4.62	6.06±0.45	17.8 <sup>+0.94</sup> <sub>-0.91</sub>	10.7±1.65	9.29±1.65	9.59±1.65	7.13

*Notes.* (1) name of galaxy, (2) luminosity in R band with unit of  $10^{10}L_\odot$  from (ATLAS<sup>3D</sup>, Cappellari et al. 2013a), (3) fitting R band mass-to-light ratio of the galaxy in dark matter halo model (4) fitting R band mass-to-light ratio of dark matter halo and the galaxy within 5 effective radii, (5) fitting R band mass-to-light ratio of the galaxy in Newtonian gravity, (6) fitting R band mass-to-light ratio of the galaxy in MONDian gravity in simple form with anisotropic parameter  $\beta$ , (7) fitting R band mass-to-light ratio of the galaxy in MONDian gravity in simple form, (8) R band mass-to-light ratio estimated from population synthesis models with Salpeter IMF (ATLAS<sup>3D</sup>, Cappellari et al. 2013b). All mass-to-light ratios are in unit of  $M_\odot/L_\odot$ . Columns (3) & (4) are the results of two-parameter fitting in Newtonian gravity (luminous mass  $M_h$  and parameter of the isothermal dark matter halo  $\sigma_v$ ). Columns (5), (6) & (7) of first four galaxies (NGC 4697, NGC 821, NGC 3379, NGC 4374) are the results of one-parameter fitting (galaxy mass  $M_h$ ). Columns (5), (6) & (7) of last five galaxies (NGC 3379, NGC 4374, NGC 5846, NGC 1344, NGC 4494) are the results of two-parameter fitting (galaxy mass  $M_h$  and SMBH mass  $M_{bh}$ ).

**Table 5.** Comparison with earlier works on NGC 3379, NGC 821 and NGC 4494.

Name	$L_B$	earlier works					present works				
		$D$ Mpc	$R_{eff}$ arcsec	$N_{PNe}$	$\Upsilon_{B,h}$ std	$\xi$	$D$ Mpc	$R_{eff}$ arcsec	$N_{PNe}$	$\Upsilon_{B,h}$ std	$\xi$
(1)	(2)	(3)	(4)	(5)	(6)	(7)	(8)	(9)	(10)	(11)	(12)
NGC 821	2.47	24	50	104	11.4	3.6	23.4	39.8	127	9.11±0.14	2.7
NGC 3379	1.56	11	35	109	4.7	5.7	10.3	39.8	214	5.71±0.05	5.1
NGC 4494	2.70	17	49	73	5.4	3.4	16.6	50	267	3.93±0.10	3.0

*Notes.* (1) name of galaxy, (2) luminosity in B band with unit of  $10^{10}L_\odot$  from Romanowsky et al. (2003), (3) distance from Romanowsky et al. (2003), (4) effective radius from Romanowsky et al. (2003), (5) total number of PNe with measured radial velocities from Romanowsky et al. (2003), (6) fitting B band mass-to-light ratio of the galaxy in MONDian gravity in standard form (Milgrom & Sanders 2003), (7) the parameter  $\xi$  of Equation (3) from Milgrom & Sanders (2003), (8) distance from ATLAS<sup>3D</sup> (Cappellari et al. 2011), (9) effective radius from ATLAS<sup>3D</sup> database (Cappellari et al. 2011), (10) total number of PNe with measured radial velocities from Coccato et al. (2009), (11) fitting B band mass-to-light ratio of the galaxy in MONDian gravity in standard form, (12) the parameter  $\xi$  of Equation (3) with mass estimated from population synthesis models with Salpeter IMF (Cappellari et al. 2013b). All mass-to-light ratios are in unit of  $M_\odot/L_\odot$ . Columns (3) to (7) are the results of earlier works (Romanowsky et al. 2003; Milgrom & Sanders 2003). Columns (8) to (12) are the results of present work.

$V^2/V_b^2$ , where  $V$  is the circular velocities by the total mass of the galaxy and  $V_b$  is the circular velocity by the baryonic mass. From the measured velocity dispersion  $\sigma_I$  at a distance  $R$  far away from the centre of galaxy, we can estimate  $V$  by putting  $g = V^2/r$  and the corresponding  $\rho = V^2/4\pi Gr^2$  into Equations (6) & (7) (with  $\beta = 0$ ) (Churazov et al. 2010).  $V_b$  is estimated by  $V_b^2 = GM_b/R$  (McGaugh 2004), and  $M_b$  is obtained by population synthesis (using Salpeter initial mass function Cappellari et al. 2013b). Figure 5 shows the mass discrepancy (represented by  $V^2/V_b^2$ ) of our sample on elliptical galaxies. This is similar to the result on spiral galaxies

(e.g., McGaugh 2004; Famaey & McGaugh 2012). Recently, Janz et al. (2016) used data from ATLAS<sup>3D</sup> and SLUGGS on the problem of mass discrepancy. Our result is consistent with theirs.

In dark matter scenario, when we use isothermal distribution for the dark matter halo and Hernquist model (with Salpeter mass) for the galaxy to fit the velocity dispersion, we get the acceleration contributed by the halo  $g_h$  and by the galaxy  $g_N$ . The result is consistent with Gentile et al. (2009), see upper panel of Figure 6. In MOND's interpretation,  $g_h = g - g_N = g(1 - \mu(g/a_o))$  (Milgrom & Sanders



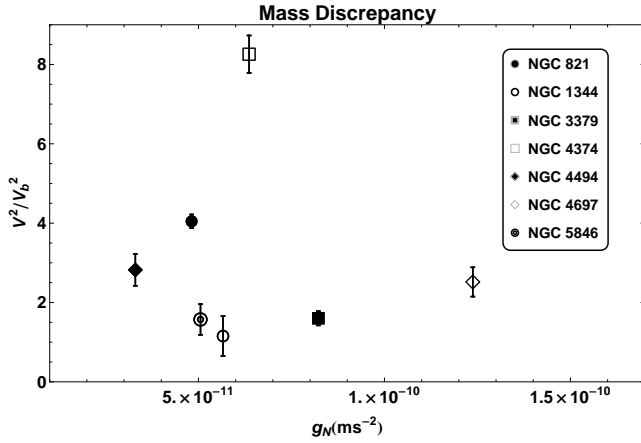


**Figure 5.** Mass discrepancy (see text for definition) is larger for smaller gravitational acceleration. Horizontal axis is the Newtonian acceleration at the location of the furthest PN by the stellar mass of the galaxy (Salpeter initial mass function is used, Cappellari et al. 2013b). Error in mass discrepancy comes from error in the velocity dispersion of PNe.

2005). We compare the prediction of MOND with the result from dark matter halo in the lower panel of Figure 6.

In summary, MOND can naturally explain the dynamics of the 7 galaxies listed in Table 1 up to 6 effective radii. Since the parameter  $\xi$  is large in these galaxies (i.e., the characteristic acceleration is large compare to  $a_0$ ), the acceleration discrepancy (or mass discrepancy) is small. MOND is close to Newtonian regime in these cases (or if dark matter halo model is used, little dark matter is needed up to several effective radii). Consequently, only slightly different results are obtained when different (inverted) interpolation functions  $\tilde{\nu}(x)$  are used. We have also considered interpolation functions other than simple form. For instances, for the standard form, the best fitted mass of a galaxy is larger than that of simple form by  $10^{+4}_{-6}\%$ . Once again, this shows that  $a_0$  is an important parameter (if not the most) to distinguish between Newtonian regime and MONDian regime (or dark matter dominated regime). It is imperative to search for high quality data for elliptical galaxies with small  $\xi$ , so that one can perform study similar to the study on HSB and LSB spiral galaxies (Sanders & McGaugh 2002).

The authors are grateful to N. Kanekar for stimulating discussion on this work and to M. Milgrom for giving many helpful comments and advices. We especially thank the anonymous reviewer for the comments and suggestions to improve our work. We also thank D. H. Hartmann and C. H. Chang for giving useful information on statistical methods of regression. This work is supported in part by the Taiwan Ministry of Science and Technology grants MOST 102-2112-M-008-019-MY3 and MOST 104-2923-M-008-001-MY3.

## REFERENCES

- Bekenstein, J. D., Milgrom, M., 1984, ApJ, 286, 7  
 Bekenstein, J. D., 2004, Phys.Rev. D70, 083509  
 Binney, J., Tremaine, S. 2008, Galactic Dynamics (2nd ed.), Chapter 4, Princeton University Press

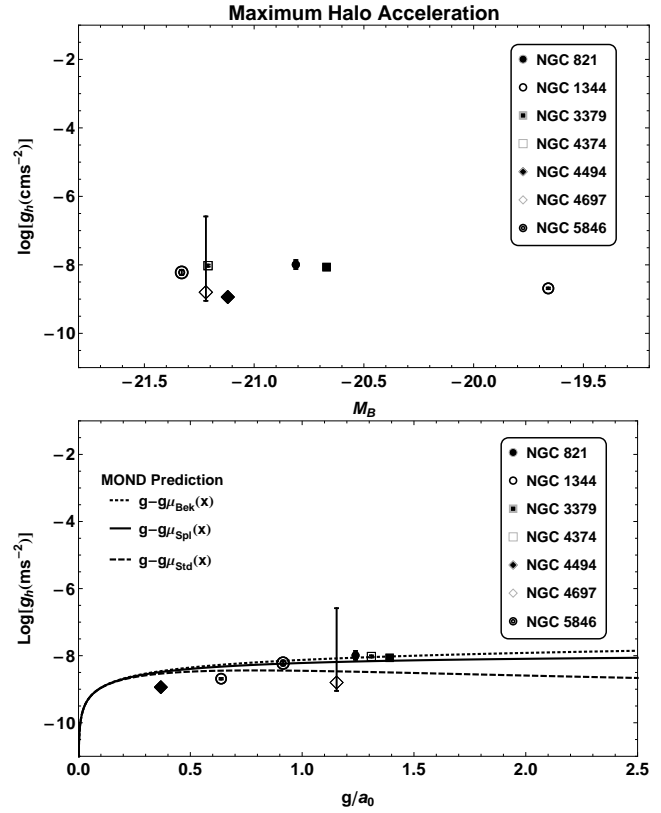


**Figure 6.** Upper panel: Maximum halo acceleration is the difference between the MONDian and Newtonian gravitational acceleration. The horizontal axis is the absolute B-band magnitude of the galaxies (see Table 1). The error in  $g_h$  comes from the error in the velocity dispersion of PNe. Except for NGC 4697, the error bar in the figure is smaller than the symbol. Lower panel: The horizontal axis is  $x = g/a_0 = (g_N + g_h)/a_0$ . The dotted line, solid line and dashed line correspond to Bekenstein form, simple form and standard form, respectively.

- Cappellari, M., Emsellem, E., Krajnovic D., McDermid R. M., et al., 2011, MNRAS, 413, 813  
 Cappellari, M., McDermid, R. M., Alatalo, K., et al., 2013a, MNRAS, 432, 1709  
 Cappellari, M., McDermid, R. M., Alatalo, K., et al., 2013b, MNRAS, 432, 1862  
 Chiu, M. C., Ko, C. M., Tian, Y., 2006, ApJ, 636, 565  
 Churazov, E., Tremaine, S., Forman, W., Gerhard, O., 2010, MNRAS, 404, 1165  
 Chiu, M. C., Ko, C. M., Tian, Y., Zhao, H. S., 2011, Phys.Rev. D83, 063523  
 Coccato, L., et al. 2009, MNRAS, 394, 1249  
 de Lorenzi, F., Debattista, V. P., Gerhard, O., et al., 2007, MNRAS, 376, 71  
 de Lorenzi, F., Gerhard, O., Coccato, L., et al., 2009, A&A, 502, 771  
 Douglas, N. G., Taylor, K., Freeman, K. G., et al., 1997, IAUS Symposium, Vol. 180, Planetary Nebulae, ed. Habing, H. J., Lamers, H. J., 493  
 Douglas, N. G., Arnaboldi, M., Freeman, K. G., et al. 2002, PASP 114, 801  
 Douglas, N. G., Napolitano, N. R., Romanosky, A. J., et al. 2007, ApJ, 664, 265  
 Famaey, B., Bruneon. J.-P., Zhao, H. S., 2007, MNRAS,

- 377, L79
- Famaey, B., Binney, J., 2005, MNRAS, 363, 603
- Famaey, B., McGaugh, S. S., 2012, Living Rev. Relativity, 15, 10
- Gentile, G., Famaey, B., Zhao, H. S., Salucci, P., 2009, Nature, 461, 627
- Hernquist, L., 1990, ApJ, 356, 359
- Hui, X., Ford, H. C., Freeman, K. C., et al., 1995, ApJ, 449, 592
- Janz, J., Cappellari, M., Romanowsky, A. J., et al., 2016, arXiv:1606.05003
- Lubin, L. M., et al., 2000, AJ, 119, 451
- Makarov, D., Prugniel, P., Terekhova, N., et al., 2014, A&A, 570, 13
- McConnell, N. J., Ma, C. P., Gebhardt, K., et al. 2011, Nature, 480, 215
- Milgrom, M., 1983, ApJ, 270, 365
- Milgrom, M., 1983, ApJ, 270, 371
- Milgrom, M., Sanders, R. H., 2003, ApJL, 599, L25
- Milgrom, M., Sanders, R. H., 2005, MNRAS, 357, 45
- Milgrom, M. 2009, Phys.Rev. D80, 123536
- Milgrom, M. 2012, Phys. Rev. Lett., 109, 131101
- McGaugh, S. S., 2004, ApJ, 609, 652
- McGaugh, S. S., 2011, Phys. Rev. Lett., 106, 121303
- Napolitano, N. R., Romanowsky, A. J., Coccato, L., et al. 2009, MNRAS, 395, 76
- Richtler, T., Schuberth Y., Hilker M., et al., 2008, A&A, 478, L23
- Riess, A. G., et al., 2011, ApJ, 730, 113
- Rodrigues, D. C., 2012, J. Cosmol. Astropart. Phys., 09, 031
- Romanosky, A. J., Douglas, N. G., Arnaboldi, M., et al., 2003, Science, 301, 1696
- Rubin, V., Fort, W. K. 1970, ApJ, 159, 379
- Samurović, S., 2012, A&A, 541, A138
- Samurović, S., 2014, A&A, 570, A132
- Samurović, S., & Ćirković, M. M., 2008, A&A, 488, 873
- Sanders, R. H., McGaugh, S. S., 2002, ARA&A, 40, 263
- Sanders, R. H., 2014, MNRAS, 439, 1781
- Schuberth Y., Richtler, T., Hilker M., et al. 2012, A&A, 544, A115
- Tian, Y., Ko, C. M., Chiu, M. C. 2013, ApJ, 770, 154
- Teodorescu, A. M., Mendez, R. H., Saglia, R. P., et al. 2005, ApJ, 635, 290
- Tian, Y., Ko, C. M., Chiu, M. C., 2013, ApJ, 770, 154
- Tortora, C., Romanowsky, A. J., Cardone, V. F. et al., 2014, MNRASL, 438, L46
- van Albada, T. S., 1982, MNRAS, 201, 939
- Zhao, H. S., Bacon, D. J., Taylor, A. N., Horne, K., 2006, MNRAS, 368, 171
- Zlosnik, T. G., Ferreira, P. G., Starkman, G. D. 2007, Phys.Rev. D75, 044017
- Zwicky, F., 1933, Helv. Phys. Acta 6, 110